JOURNAL OF AIRCRAFT
Vol. 39, No. 1, January–February 2002

Wavelet Approach to Flutter Data Analysis

W. J. Staszewski*
University of Sheffield, Sheffield, England S1 3JD, United Kingdom
and
J. E. Cooper†
University of Manchester, Manchester, England M13 9PL, United Kingdom

A wavelet-based method is presented to analyze flight flutter test data. The procedure utilizes the filter action of the continuous wavelet transform to enable damping estimation. An indication of the overall stability is obtained from changes in the shape of the wavelet transform amplitude cross sections. The method is illustrated using simple simulated examples and real flight-test data. A good agreement was achieved compared to classical parameter estimation techniques.

Nomenclature

$[A]$	=	structural inertia matrix
$A(t)$	=	envelope function
a	=	dilation (scale)
$[B]$	=	aerodynamic damping matrix
b	=	translation
$[C]$	=	aerodynamic stiffness matrix
C_g	=	admissibility constant
c	=	damping
$[D]$	=	damping matrix
$[E]$	=	stiffness matrix
$\boldsymbol{F}$	=	excitation vector
f	=	frequency
f_c	=	wavelet central frequency
f_h	=	shift frequency
f_s	=	signal sampling frequency
f_w	=	wavelet sampling frequency
f_0	=	Morlet function parameter
$G(f)$	=	Fourier transform of $g(t)$
$g(t)$	=	wavelet function
$g_{a,b}(t)$	=	dilated and translated wavelet function
j	=	$\sqrt{-1}$
$[K]$	=	stiffness matrix
k	=	stiffness
$[M]$	=	inertia matrix
m	=	mass
S	=	shape parameter
t	=	time
t_c	=	time centroid
v	=	airspeed
$(W_g x)$	=	continuous wavelet transform
X	=	Fourier transform of x
$x(t)$	=	time-domain signal
Δf	=	analyzing function bandwidth
Δf_g	=	wavelet bandwidth
Δt	=	analyzing function duration
Δt_g	=	wavelet duration
ζ	=	damping ratio
ρ	=	air density
$\phi(t)$	=	instantaneous phase
ω_n	=	natural frequency
$*$	=	complex conjugate

Received 26 April 1999; revision received 28 November 2000; accepted for publication 27 March 2001.

*Lecturer, Dynamics Research Group, Department of Mechanical Engineering, Mappin Street; w.j.staszewski@sheffield.ac.uk.

†Senior Lecturer, School of Engineering, Oxford Road; j.e.cooper@man.ac.uk.

I. Introduction

FLUTTER is one of the most important aeroelastic phenomena. It is a violent instability in which the structure extracts energy from the airstream, often resulting in structural failure. Flutter occurs when the aerodynamics forces associated with two or more modes of vibration couple in an unfavorable manner. There are various types of flutter; however, the greatest effort in the design and certification process is addressed toward linear flutter in the unseparated flow case.

For this flight regime, the behavior of the aircraft in flight can be described by a second-order differential equation of the form

$$[A]\ddot{y} + (\rho V[B] + [D])\dot{y} + (\rho V^2[C] + [E])y = 0 \qquad (1)$$

In practice, $[B]$ and $[C]$ depend on unsteady aerodynamics, which means that they are functions of the frequency of vibration, as well as the airspeed, altitude, and wing dimensions. The system given by Eq. (1) possesses frequencies and damping ratios in the same manner as a system with no aerodynamic terms. However, these parameters change as the flight condition alters.

Classical binary flutter consists of two modes, often wing bending and torsion, whose damped natural frequencies of vibration become closer as the airspeed increases. As the critical speed is approached, one of the damping ratios increases, whereas the other decreases rapidly to zero. Beyond this critical speed (the flutter speed), this second damping ratio becomes negative, and any small displacement will result in a divergent unstable oscillation.

The airworthiness clearance procedure[1,2] on all new and modified aircraft involves ground vibration testing to validate the structural finite element models and wind-tunnel testing to validate the aerodynamic models. Finally, flight flutter tests have to be carried out to demonstrate freedom from flutter over the entire flight envelope. Civil prototype aircraft must typically be flutter free to a speed of 20% greater than the design dive speed.

The conventional flutter test[1,2] consists of flying the aircraft at a desired flight condition and then measuring the response to some form of excitation. These data are then curve fitted to estimate frequencies and damping ratios. From the trends of these parameters against speed, or Mach number, the decision is then made as to what new test condition to fly at. Flight flutter tests are also very costly and time consuming. They usually combine flight conditions involving different fuel loads, flight control gains, flight speeds, and other important parameters.

It is well known that damping parameters are the most difficult to estimate accurately, and the analysis of flight flutter data is much more difficult[2,3] than that of ground vibration testing due to the noisy environment, time constraints, and problems with instrumenting the aircraft. Despite these difficulties, the estimates of damping parameters must be accurate and reliable to ensure a safe clearance program. This is not an easy task. Damping estimates in flutter tests are usually obtained using conventional frequency- and time-domain modal parameter estimation methods.[3] Recent applications have also included the use of the Hilbert transform (see Ref. 4), spatial filtering,[5] and wavelets.[6]

The aim of this paper is to apply previous work on wavelet-based analysis[6] to flight flutter testing. A brief introduction to the continuous wavelet transform is given followed by a description of the damping estimation procedure based on the wavelet transform cross sections, including an approach using the envelope function. These theoretical developments are initially demonstrated using a simple multi-degree-of-freedom (MDOF) example. Results using the approach are then compared with those results obtained using conventional analysis approaches on simulated and real flight-test data.

II. Continuous Wavelet Transform

The Fourier transform can be considered as a decomposition of a function into a linear combination of harmonics weighted by Fourier coefficients. This decomposition does not give any local information about the function due to the infinite nature of the trigonometric functions used in the analysis. A localized decomposition can be obtained using the wavelet transform. A brief introduction to the relevant wavelet theory is given in this section. More detailed analysis can be found elsewhere.[7]

A. Definition

For all functions $x(t)$ satisfying the condition

$$\int_{-\infty}^{+\infty} |x(t)|^2 \, \mathrm{d}t < \infty \tag{2}$$

[which implies that $x(t)$ decays to zero at $\pm\infty$], the wavelet transform can be defined as

$$(W_g x)(a, b) = \frac{1}{\sqrt{a}} \int_{-\infty}^{+\infty} x(t) g^* \left(\frac{t-b}{a} \right) \mathrm{d}t \tag{3}$$

where b is a translation indicating the locality, a is a dilation or scale parameter, and $g(t)$ is an analyzing (basic) wavelet. Each value of the wavelet transform $(W_g x)(a, b)$ is normalized by the factor $1/\sqrt{a}$. This normalization ensures that the integral energy given by each wavelet $g_{a,b}(t)$ is independent of the dilation a.

Any function $g(t)$ can be used as an analyzing wavelet when it satisfies the admissibility condition[7]

$$C_g = \int_{-\infty}^{+\infty} \frac{|G(f)|^2}{|f|} \, \mathrm{d}f < \infty \tag{4}$$

where $G(f)$ is the Fourier transform of $g(t)$; $g(t)$ must be also a window function to enable the possibility of time-frequency localization. This additionally means that

$$\int_{-\infty}^{+\infty} |g(t)| \, \mathrm{d}t < \infty \tag{5}$$

In practice, some regularity and smoothness of the wavelet function is also imposed. A number of different functions have been used in the wavelet analysis. In what follows, the Morlet wavelet, defined in the time domain as[8]

$$g(t) = \exp(j 2\pi f_0 |t|) \exp[-(|t|^2/2)] \tag{6}$$

is applied. The Morlet wavelet can be represented in the frequency domain as a shifted Gaussian function

$$G(f) = \sqrt{2}\pi \exp\left[-2\pi^2 (f - f_0)^2\right] \tag{7}$$

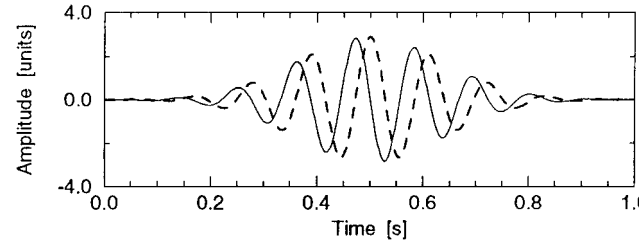

a) Time domain, dilation 0.4

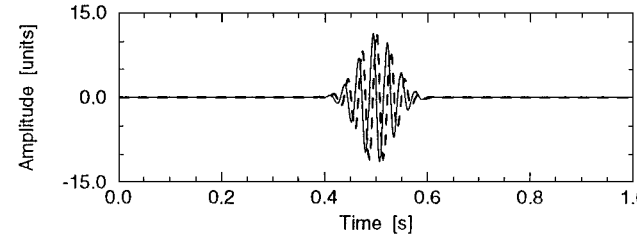

b) Time domain, dilation 0.1

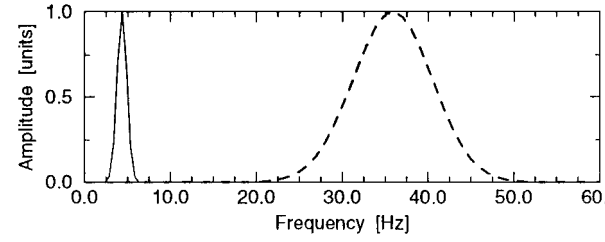

c) Frequency domain

Fig. 1 Morlet wavelet function:——, real part; - - -, imaginary part; ——, dilation – 0.4; and - - -, dilation – 0.1.

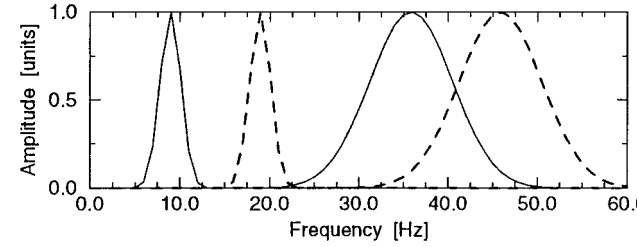

Fig. 2 Shifted Morlet wavelet function: ——, Morlet wavelet; and - - -, shifted Morlet wavelet: a) time domain and b) frequency domain.

The admissibility condition given by Eq. (4) is not satisfied because $G(0) \geq 0$, which gives $C_g = +\infty$. In practice the value of $f_0 > 5$ is used,[8] which meets, approximately, the requirements given by Eq. (4). Figure 1 shows an example of the Morlet wavelet function in the time and frequency domain for different values of dilation parameters.

In many cases the so-called shifted Morlet wavelet can be used. Thus, instead of f in Eq. (7), $(f - f_h)$ is applied, where f_h is the shift frequency. When the shifted Morlet wavelet is used, the frequency position of the wavelet function is changed, but its frequency bandwidth remains unchanged, giving a better time resolution. This effect can be seen in Fig. 2.

In summary, the wavelet transform is an example of a linear transformation that decomposes an arbitrary function $x(t)$ into elementary functions $g_{a,b}(t)$, which are obtained from the analysing wavelet $g(t)$ by dilation and translation. The time decomposition is given by translation b. The frequency segmentation, that is, scale decomposition, is obtained by dilating the chosen analyzing wavelet. These two operations produce a basis that can represent any reasonable function. For practical purposes, the decay given by Eq. (2) is very fast and, thus, introduces locality into the analysis. This is not the case of the Fourier transform, where one infinite trigonometric function gives a global representation.

B. Properties

The wavelet transform has a number of useful properties.[7] A summary of the most important time-frequency localization properties used in the paper is given next.

The wavelet transform is a linear decomposition of a signal. For N given functions x_i and N complex values α_i, $i = 1, 2, \ldots, N$,

$$\left(W_g \sum_{i=1}^{N} \alpha_i x_i\right)(a, b) = \sum_{i=1}^{N} \alpha_i (W_g x_i)(a, b) \tag{8}$$

which shows why the wavelet analysis is convenient for multicomponent signals.

It is clear from the definition that, whereas the Fourier transform extracts periodic infinite waves from the analyzed function, the wavelet transform analyzes a function only locally at windows defined by a wavelet function. On first inspection, Eq. (3) is in general nonlocal. The value of $(W_g x)(a, b)$ at a point (a_0, b_0) depends on $x(t)$ for all t. However, the conditions given by Eqs. (2) and (5) provide that the function $g(t)$ decays to zero at $-\infty$ and $+\infty$. If one assumes a fast decay, that is, the values of $g(t)$ are negligible outside the interval $(t_{\min}, t_{\max})$, the transform becomes local.[7]

The frequency localization is clearly seen when the wavelet transform is expressed in terms of the Fourier transform

$$(W_g x)(a, b) = \sqrt{a} \int_{-\infty}^{+\infty} X(f) G^*_{a,b}(af) \exp(i2\pi f b)\, \mathrm{d}f \tag{9}$$

This localization depends on the dilation parameter a. The local resolution of the wavelet transform in time and frequency is determined by the duration and bandwidth of analyzing functions[7]

$$\Delta t = a \Delta t_g \qquad \Delta f = \Delta f_g / a \tag{10}$$

where Δt_g and Δf_g are the duration and bandwidth of the basic wavelet function, respectively. Thus, in the frequency domain, the wavelet transform has good resolution at low frequencies, and conversely, good resolution at high frequencies in the time domain. The latter case being suitable for non-stationary and transient signal detection.

The wavelet transform decomposes the signal in the timescale domain. The relationship between the scale and frequency representations[9] is illustrated here using the Morlet analysing wavelet function. The bell-shaped Morlet wavelet filter given by Eq. (7) can be approximated using the triangle function[10]

$$G(f) = \begin{cases} 1 - \dfrac{2\pi |af - f_0|}{\sqrt{\pi}} & 2\pi |af - f_0| \le \sqrt{\pi} \\ 0 & 2\pi |af - f_0| \ge \sqrt{\pi} \end{cases} \tag{11}$$

The wavelet filter central frequency and bandwidth follow from this approximation as

$$f_c = f_0 / a \tag{12}$$

and

$$\Delta f = \sqrt{\pi} / \pi a \tag{13}$$

respectively. It is clearly seen that both filter parameters depend on dilation a. Equation (12) gives also the relationship between the scale parameter and frequency of the wavelet analysis for the Morlet wavelet function. In general, the sampling frequency of the wavelet f_w and the sampling frequency of the signal f_s do not need to be equal. As a consequence, Eq. (12) can be modified[9] as

$$f_c = (f_0 / a) f_s / f_w \tag{14}$$

C. Numerical Implementation

The wavelet transform can be calculated numerically in the time or frequency domain using Eqs. (3) or (9), respectively. The frequency-domain approach is straightforward and leads to the interpretation of the calculation algorithm as a bank of filters. Equation (9) can be written in discrete form as

$$W(m, n) = \sqrt{m \Delta a} \sum_{f_n} X(f_n) G^*(m \Delta a f_n) \exp(i2\pi f_n n \Delta b) \tag{15}$$

where f_n are discrete values of frequency and Δa and Δb are the increments of dilation and translation, respectively. It is clearly seen from this equation that the wavelet transform can be implemented with the help of the fast Fourier transform (FFT) algorithm. This operation can be performed by generating the family of all dilated wavelets in the frequency domain and multiplying $G^*(m \Delta a f_n)$ by $X(f_n)$ before transforming the results back to the time domain using the inverse FFT.

Because the wavelet transform is complex valued, it can be presented in terms of its amplitude and phase. It is usual to normalize the maximum values of the modulus to 1.0, with the phase values distributed between 0 and 2π. To further enhance the interpretation of the phase plots, if the modulus of the wavelet transform is less than 3% of its maximum value, the phase value is not plotted. A logarithmic scale on the dilation axis is chosen to enhance the small dilation coefficients. Simple examples of the use of the method may be found in Ref. 11.

III. Wavelet Decomposition for Damping Estimation

A number of different techniques have been proposed recently to estimate damping using wavelets.[11] These procedures are based on 1) wavelet transform cross sections, 2) wavelet domain filtering and impulse response functions, and 3) wavelet ridges and skeletons. Here, the procedure based on wavelet transform cross sections is presented. This procedure is used in the paper to estimate the damping in the flutter vibration data examples.

A. Mode Decoupling

The MDOF system is governed by the general equation

$$[M]\ddot{X} + [C]\dot{X} + [K]X = \boldsymbol{F} \tag{16}$$

which is a set of N coupled equations. The impulse response of this MDOF system can be given in general form as

$$h(t) = \sum_{i=1}^{N} A_i \exp(-\xi_i \omega_{n_i} t) \sin\left(\sqrt{1 - \xi_i^2}\, \omega_{n_i} t + \varphi_i\right) \tag{17}$$

where ω_{ni} is the natural frequency, N is the number of considered modes, A_i is the residue magnitude of the ith mode, and ξ_i is the damping ratio. This response is a linear combination of single modal components; each mode is given by an exponentially decaying harmonic function. Only a few methods exist that enable the modes to be uncoupled, for example, modal filtering[12] and complex envelope.[13] More recently, the wavelet transform has been used for mode decoupling.

Section II showed that the wavelet transform decomposes the analyzed signal as a time–frequency filter. Because wavelets are localized in time and frequency, Equations (3) and (9) can be rewritten for multicomponent signals as

$$\left(W_g \sum_{i=1}^{N} x_i\right)(a, b) = \frac{1}{\sqrt{a}} \sum_{i=1}^{N} \int_{t - a\Delta t_g}^{t + \Delta t_g} x_i(t) g \times \left(\frac{t - b}{a}\right) \mathrm{d}t \tag{18}$$

and

$$\left(W_g \sum_{i=1}^{N} x_i\right)(a, b) = \sqrt{a} \sum_{i=1}^{N} \int_{f_i - (\Delta f_g / a)}^{f_i + (\Delta f_g / a)} X(f) G^*_{a,b}(af) \times \exp(i2\pi f b)\, \mathrm{d}f \tag{19}$$

respectively. This shows clearly the filtering action of the wavelet transform where the wavelet analyzing function for each mode is peaked at modal frequency f_i. For the Morlet wavelet function, the relationship between frequency and dilation and the frequency bandwidth of the filter is given by Eqs. (12) and (13), respectively.

B. Damping Estimation Procedure

It is well known that the dissipative mechanism of the system can be detected by the analysis of the decaying envelope $A(t)$ of the impulse response function. For a single mode in Eq. (17), the constitutive function $A(t)$ is written in the explicit form

$$A(t) = A_0 \exp[(-c/2m)t] \tag{20}$$

where $c = \xi/2\sqrt{(km)}$. The envelope function $A(t)$ can be obtained using the complex envelope approach based on the Hilbert transform (see Ref. 13) Taking the logarithm of Eq. (20) gives

$$\ln A(t) = -\xi\omega_n t + \ln A_0 \tag{21}$$

Thus, the damping ratio ξ of the system can be estimated from the slope of the straight envelope line $A(t)$ plotted on a semilogarithmic scale. This procedure is well known in the literature, and applications can be found elsewhere.[14,15] A similar procedure can be applied in the case of the wavelet transform.[11] For the underdamped case, the solution for a single mode of the system can be given in the form

$$x(t) = A(t) \exp[\phi(t)] \tag{22}$$

where $A(t)$ is assumed to be a slowly varying function. For the Morlet wavelet function $g(t)$ given by Eq. (7), which is also the analytic complex valued function and has good localization properties in the frequency domain, the wavelet transform of the solution given by Eq. (22) can be approximated as[16]

$$(W_g x)(a, b) \approx A(b) G^*(a\dot{\phi}(b)) \exp[j\phi(b)] + \mathcal{O}(|\dot{A}|, |\ddot{\phi}|) \tag{23}$$

where $G(\cdot)$ is the frequency representation of the Morlet wavelet function. The modulus of this function is given by

$$|W_g x)(a, b)| \approx A(b) |G^*[a\dot{\phi}(b)]| \tag{24}$$

For a single-mode constitutive envelope and instantaneous functions taken from Eq. (17), this can be represented as

$$|(W_g x)(a_0, b)| \approx A_0 \exp(-\xi\omega_n b) \left| G^*\left(a_0 \pm j\omega_n\sqrt{1-\xi^2}\right)\right| \tag{25}$$

for the given value of dilation a_0. The value of dilation a_0 can be related to the natural frequency of the system f_0 through Eq. (12) or (14). Equation (25) reveals that

$$\ln|(W_g x)(a_0, b)| \approx -\xi\omega_n b + \ln\left(A_0 \left| G^*\left(a_0 \pm j\omega_n\sqrt{1-\xi^2}\right)\right|\right) \tag{26}$$

and thus, the damping ratio ξ of the system can be estimated from the slope of the straight line obtained by plotting the log of the wavelet modulus cross section $|(W_g x)(a_0, b)|$. This result is similar to the envelope analysis given by Eq. (21). The result given by Eq. (26) was obtained also on assumption that the analyzing wavelet function has good localization properties in the frequency domain. In practice when the cross section of the wavelet transform is used for the particular value of dilation a_a, the Fourier transform of the Morlet wavelet function is peaked at the value of frequency f_0; both values are related by Eq. (12). Note that the cross section of the wavelet transform in the scale domain can be obtained directly from Eq. (15) without any calculation of the whole timescale plane. One can see that the procedure based on the wavelet transform is very similar to the procedure based on the classical complex envelope function. The advantage over the classical procedure is the wavelet filtering or decoupling action.

C. Shape Parameter

The shape of the cross section of the wavelet transform can give information about the decay amplitude of the signal, which can indicate the damping or stability of the system. Many parameters exist that can be used to study the decaying nature of the amplitude. The length of the decay, which indicates the amount of overall damping, can be measured using the shape parameter[4]

$$S = 1/t_c \tag{27}$$

where t_c is the time centroid of the wavelet cross section envelope. It can be defined as

$$t_c = \frac{\int_0^{b\,\max} (W_g x)(a, b) b \, \mathrm{d}b}{\int_0^{b\,\max} (W_g x)(a, b) \, \mathrm{d}b} \tag{28}$$

where $b_{\max}$ is the maximum value of time chosen to give an upper bound to the analyzed area. For an underdamped response, a decrease in S indicates a decrease in the system damping. It may be shown that, for a single DOF system, when the damping goes to zero, then S goes to $2/b_{\max}$. This limit gives a threshold for system instability. The shape parameter S of the wavelet cross section does not identify the damping of the system; however, it can be used as an approximate measure of the overall system damping.

D. Example

As an example of the use of the proposed approach, a two-DOF system with well-separated and closely spaced modes is analyzed. The parameters of the systems are as follows: $f_1 = 20$ Hz, $f_2 = 75$ Hz, $\xi_1 = 0.03$, and $\xi_2 = 0.045$ for the well-separated modes system and $f_1 = 25$ Hz, $f_2 = 30$ Hz, $\xi_1 = 0.06$, and $\xi_2 = 0.02$ for the closely spaced modes system (although they may not seem to be closely spaced, there is significant interaction between the modes). Figures 3 and 4 show the impulse and frequency response of the system, respectively. The wavelet transform for the system with closely spaced modes is given in Figs. 5a and 5b. It is difficult to see both modes in this case. However, these modes can be separated using the proper values of dilation and the shifted Morlet wavelet function, as shown in Figs. 5c and 5d. The cross sections of the wavelet transform amplitude for the system with close modes are presented in Fig. 6. These cross sections were plotted in the semilogarithmic scale in Fig. 7 and used to obtain the damping values and shape parameters given in Table 1. It can be seen that good estimates of damping parameters were obtained.

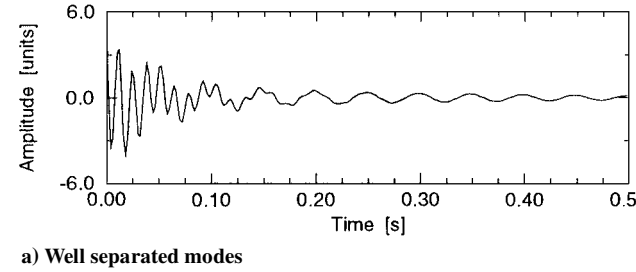

a) Well separated modes

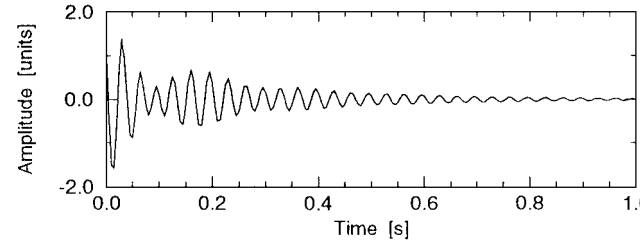

b) Close modes

Fig. 3 Impulse response functions for the two-DOF example.

Table 1 Damping estimates for the analyzed binary system

Frequency, Hz	True damping ratio	Estimated damping ratio	Error, %	Shape parameter
20	0.03	0.02987	−0.43	5.11
75	0.045	0.04489	−0.24	17.53
25	0.06	0.06062	+1.03	6.22
30	0.02	0.01998	−0.1	3.71

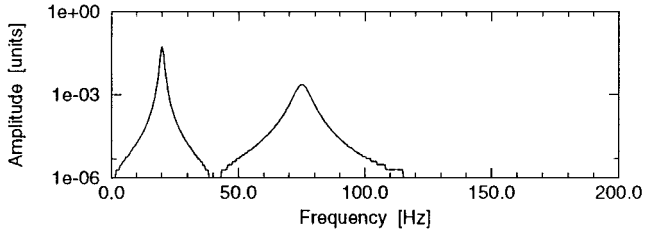

a) Well separated modes

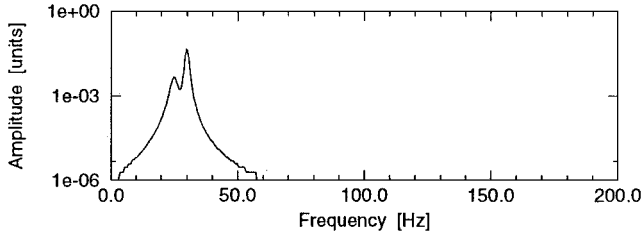

b) Close modes

Fig. 4 FRF amplitudes for the two-DOF example.

IV. Flutter Data Analysis

The damping identification methods based on the wavelet transform cross sections were applied to simulated and industrial aircraft flight-test data.

A. Simulated Binary Flutter Data

Impulse response data was generated at different flight speeds using a simulated binary aeroelastic system. The frequency, damping, and airspeed parameters were chosen to match classical wing bending/torsion vibration. The generated data were corrupted by a Gaussian noise (signal-to-noise ratio $= 8$ dB). Damping ratios were estimated using the wavelet transform approach described earlier.

Figure 8 shows a comparison between the theoretical and estimated values of damping ratio for two simulated modes. It can be seen that satisfactory estimation of damping was obtained. The shape parameters of the wavelet transform cross sections were then calculated. The variation of shape parameters with speed are presented in Fig. 9. Here the condition of zero damping corresponds to the shape parameter equal to 0.125 ($b_{\max} = 16$ s). When Figs. 8 and 9 are compared, a good correlation between damping ratios and shape parameters can be observed.

B. Flight-Test Data

The wavelet transform approach was also applied to flight-test data. The data sets were taken from the flight flutter test of a commercial aircraft. Impulse response functions were obtained from the estimated frequency response functions (FRFs) for two different flight speeds.

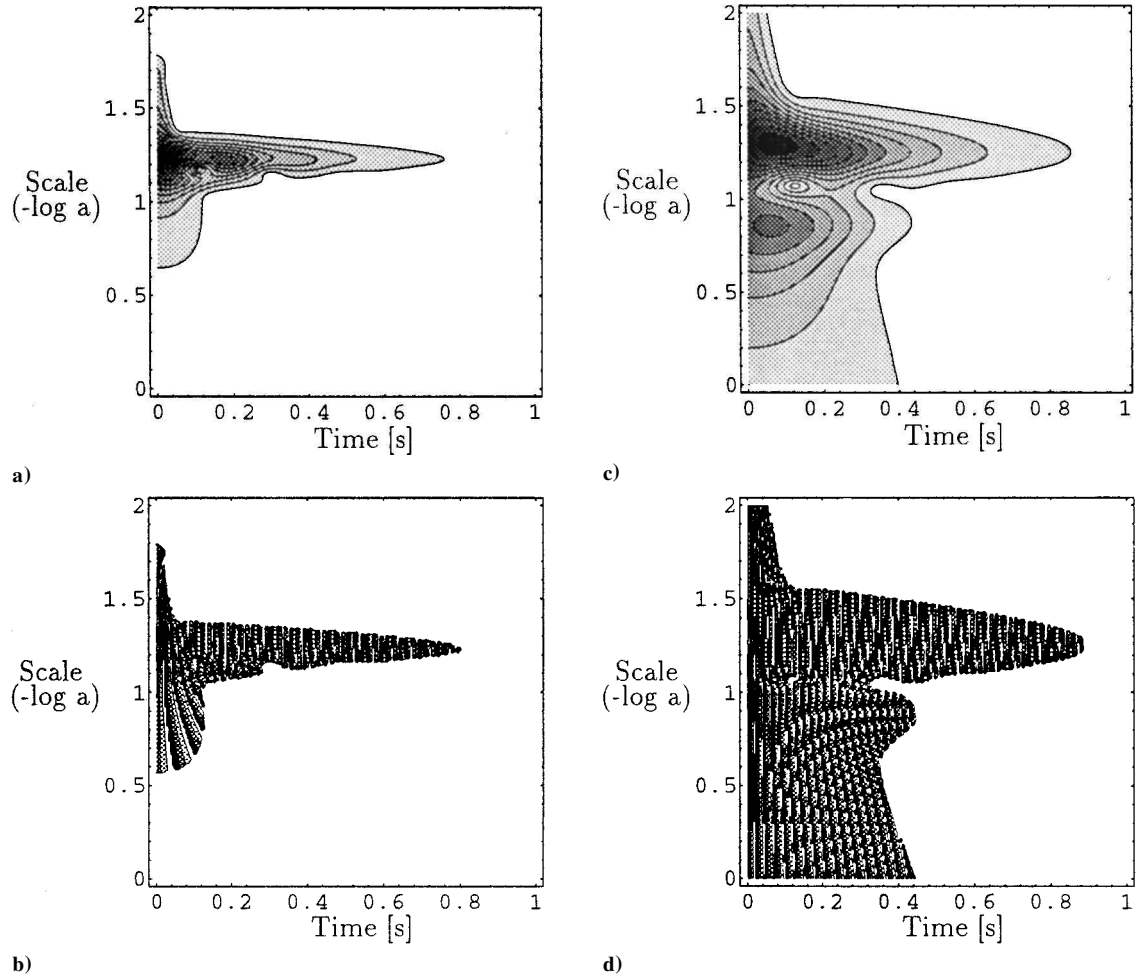

Fig. 5 Wavelet transform for the two degree-of-freedom example: a) Morlet wavelet function used, amplitude; b) Morlet wavelet function used, phase; c) shifted Morlet wavelet function used, amplitude; and d) shifted Morlet wavelet function used, phase.

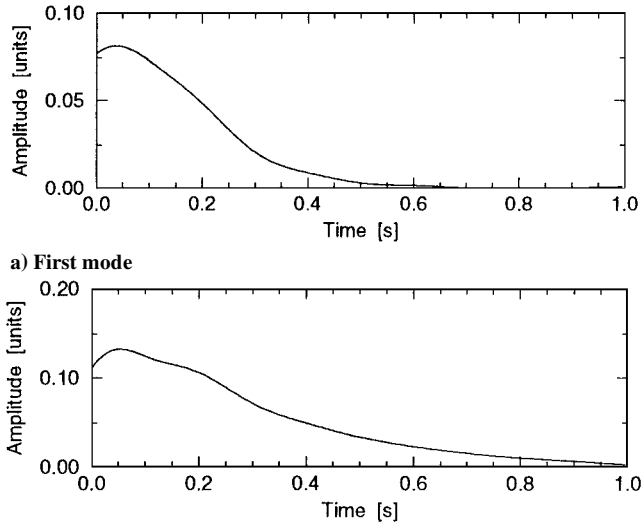

Fig. 6 Cross sections of the wavelet transform amplitude presented in Fig. 5.

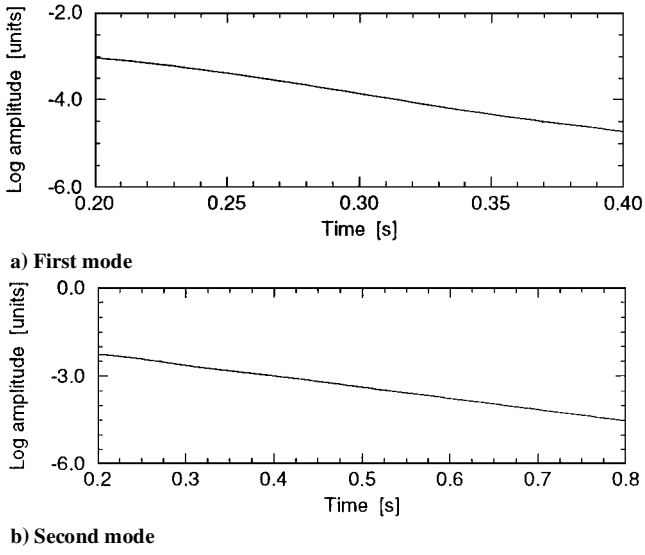

Fig. 7 Semilogarithmic plot of the cross sections shown in Fig. 5.

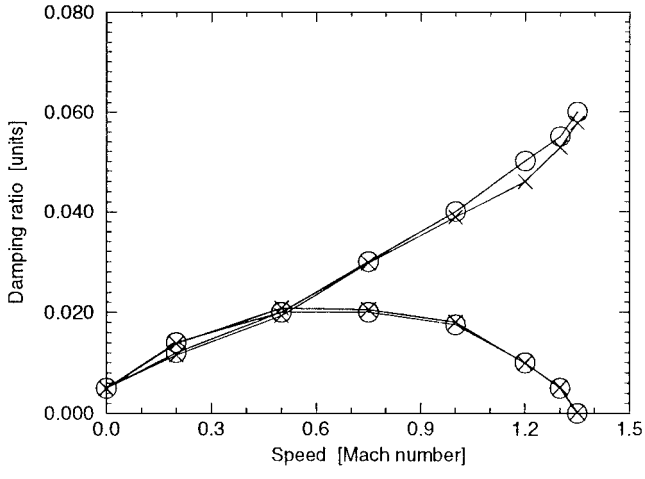

Fig. 8 Binary flutter example; variation of damping with speed: o, theroy, and ×, wavelet transform.

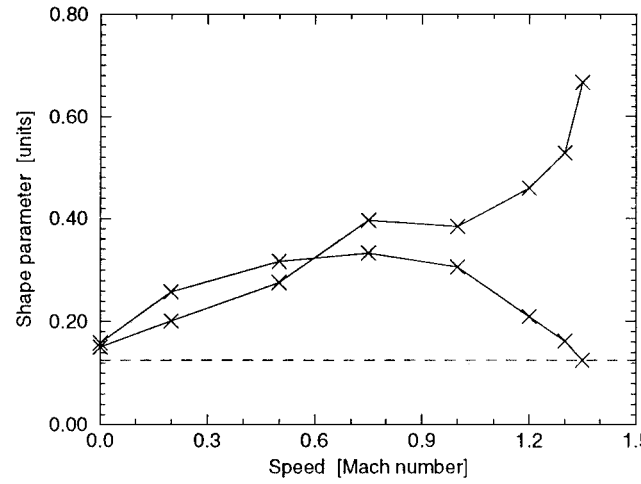

Fig. 9 Binary flutter example; variation of shape parameters with speed.

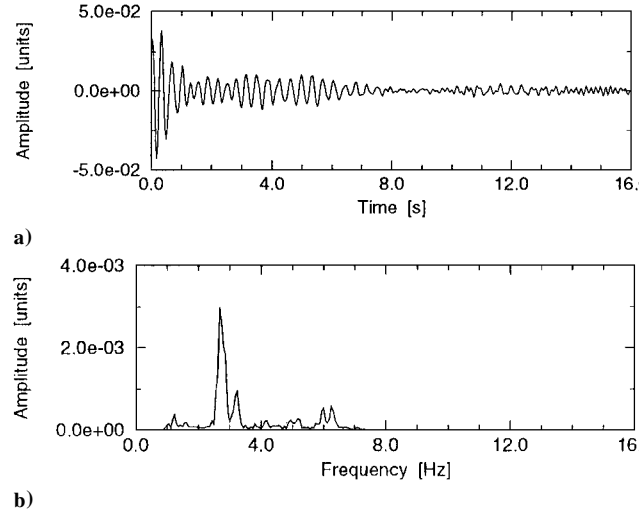

Fig. 10 Flight flutter data: a) impulse response and b) FRF amplitude.

Figures 10a and 10b show an example of the impulse response and the FRF amplitude, respectively, for the data representing the lower flight speed. The impulse responses were analyzed using the wavelet-based procedures. Figure 11 shows an example of the wavelet transform for the data presented in Fig. 10a. It can be seen that the proper choice of wavelet parameters allows one to focus the analysis on the chosen modes. The wavelet transform cross sections for these modes are presented in Fig. 12. For this work, it was decided to analyze the two dominant modes at each flight speed. A drop in the amplitude of the wavelet cross section representing the first mode, at about 2.5 s, can be observed in Fig. 12a. This effect is due to the interaction between the closely spaced modes; the first mode has not been isolated effectively. The effect is much less pronounced for the second mode.

The damping ratios can be still estimated using the semilogarithmic plots given in Fig. 13. A linear curve-fitting procedure was used to obtain the slope. The values of shape parameters were calculated for the cross sections given in Fig. 12. The estimated frequency, damping, and shape parameters values for two different flight speed are shown in Table 2. Here the results are compared with two conventional time-domain system identification methods, namely, the least-squares complex exponential and smith least-squares algorithms (see Ref. 3). It can be seen that there is a good agreement between the results obtained using all methods. The shape parameters increase monotonically with the change of damping and, thus, also give the indication of the decrease in the damping.

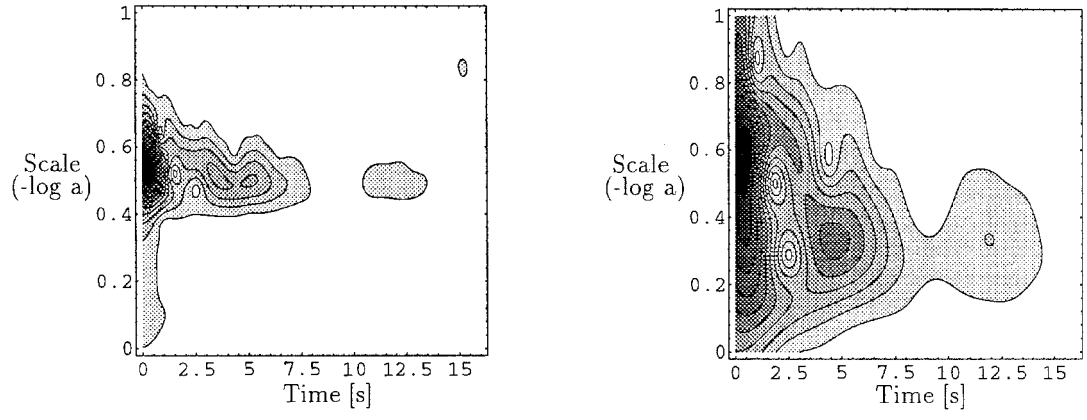

Fig. 11 Wavelet transform amplitude for the flight flutter data.

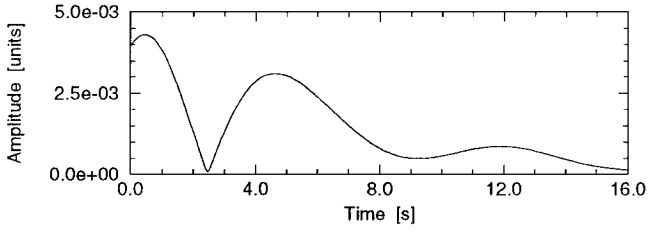

a) First mode

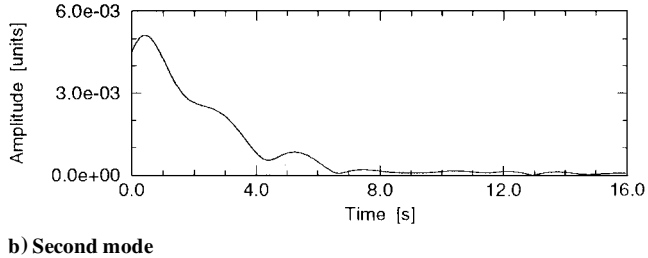

b) Second mode

Fig. 12 Wavelet transform amplitude cross sections for the flight flutter data.

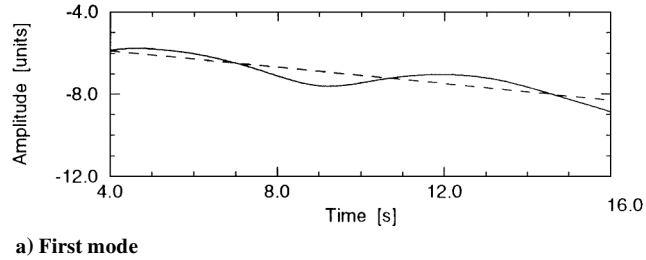

a) First mode

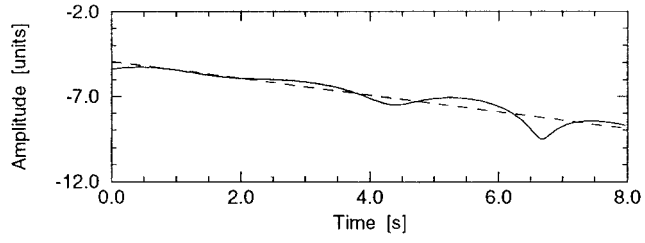

b) Second mode

Fig. 13 Semilogarithmic plots for the wavelet transform amplitude cross sections.

Table 2 Estimated damping ratios for the flight flutter data

Flight speed	Frequency, Hz	Damping ratio ξ SLS	LSCE	Wavelets	Wavelet shape parameter
Low	2.69	0.0140	0.0264	0.0120	0.195
Low	3.25	0.0242	0.0267	0.0242	0.389
High	2.69	0.0081	0.0133	0.0088	0.174
High	2.88	0.0068	0.0073	0.0067	0.166

V. Conclusions

A wavelet method suited for the analysis of flutter data has been presented. The method uses changes in the shape of the continuous wavelet transform cross section to allows the user to get a measure in the overall change of stability. Similar damping estimates were obtained on simulated and real flutter test data sets compared to conventional curve-fitting methods. The examples highlight the ability to use the wavelet transform to highlight modes of interest. The procedure presented is relatively simple but is seen as complementing rather than replacing existing techniques. Further work with either real flight or wind-tunnel data is required to fully evaluate the procedure, in particular for the application to time-varying systems.

References

[1]Kehoe, M. W., "A Historical Overview of Flight Flutter Testing," AGARD Paper 1, May 1995.

[2]Wright, J. R., "Flight Flutter Testing," Lecture Series on Flutter of Winged Aircraft, Von Kármán Inst., Vol. VKI LS, Rhode-Saint-Geneśe, Belgium, 1991.

[3]Cooper, J. E., "Parameter Estimation Methods for Flight Flutter Testing," AGARD Paper 10, 1995.

[4]Cooper, J. E., Emmett, P. R., Wright, J. R., and Schofield, M. J., "Envelope Function: A Tool for Analyzing Flutter Data," *Journal of Aircraft*, Vol. 30, No. 5, 1993, pp. 785–790.

[5]Shelley, S. J., and Pickrel, C. R., "New Concept for Flight Flutter Parameter Estimation," *Proceedings of the 15th International Modal Analysis Conference*, Vol. 1, Orlando, FL, 1997, pp. 490–496.

[6]Staszewski, W. J., and Cooper, J. E., "Flutter Daya Analysis using the Wavelet Transform," *Proceedings of the International Congress MV2: New Advances in Modal Synthesis of Large Structures, Non-Linear, Damped and Non-Deterministic Cases*, Lyon, France, 1995, pp. 549–561.

[7]Mallat, S., "A Wavelet Tour of Signal Processing," *Wavelets: A Tutorial in Theory and Applications*, Academic, San Diego, CA, 1998.

[8]Kronland-Martinet, R., and Mortlet, J., "Analysis of Sound Throught Wavelet Transforms," *International Journal of Pattern Recognition and Artificial Intelligence*, Vol. 1, No. 2, 1987, pp. 273–302.

[9]Staszewski, W. J., and Tomlinson, G. R., "Application of the Wavelet Transform to Fault Detection in a Spur Gear," *Mechanical Systems and*

Signal Processing, Vol. 8, No. 3, 1994, pp. 289–307.

[10]Harris, J. W., and Stocker, H., *Handbook of Mathematics and Computational Science*, Springer-Verlag, New York, 1998, Chap. 11.

[11]Staszewski, W. J., "Identification of Damping in MDOF Systems using Time-Scale Decomposition," *Journal of Sound and Vibration*, Vol. 203, No. 2, 1997, pp. 283–305.

[12]Brancaleoni, F., Spina, D., and Valente, C., "A Free Oscillation Based Technique for the Identification of Non-Linear Dynamic Systems," *Computational and Applied Mechanics I—Algorithms and Theory*, edited by C. Brezinski and U. Kulish, Elsevier, Amsterdam, 1992.

[13]Randall, R. B., "Frequency Analysis," Bruel and Kjaer Application Note, Naerum, Denmark, 1987.

[14]Jones, D. I. G., "Application of Damping Treatments," *Shock and Vibration Handbook*, 3rd ed., edited by C. M. Harris, McGraw–Hill, New York, 1987, Chap. 37.

[15]Brancaleoni, F., Spina, D., and Valente, C., "Damage Assessment from the Dynamic Response of Deteriorating Structures," *Safety Evaluation Based on Identification Approaches*, edited by H. G. Natke, G. R. Tomlinson, and J. T. P. Yao, Vieweg, Braunschweig/Wiesbaden, Germany, 1993, pp. 276–291.

[16]Carmona, R. A., Hwang, W. L., and Torrsani, B., "Characterization of Signals by the Ridges of their Wavelet Transforms," *IEEE Transactions on Signal Processing*, Vol. 45, No. 10, 1997, p. 2586.